Applied Catalysis B: Environmental 152–153 (2014) 19–27

Contents lists available at ScienceDirect

Applied Catalysis B: Environmental

journal homepage: www.elsevier.com/locate/apcatb

Sustainable syngas production from ethylene glycol reforming processes using Rh-based catalysts in microreactors

U. Izquierdo[a,*], M. Wichert[b], V.L. Barrio[a], G. Kolb[b]

[a] Faculty of Engineering, University of the Basque Country, Bilbao, Spain
[b] Institut für Mikrotechnik Mainz GmbH (IMM), Mainz, Germany

ARTICLE INFO

Article history:
Received 12 July 2013
Received in revised form
18 December 2013
Accepted 9 January 2014
Available online 19 January 2014

Keywords:
Ethylene glycol
Steam reforming
Hydrogen
Rhodium
Micro reactor

ABSTRACT

In this work the ethylene glycol (EG) as feed for syngas production by steam reforming (SR) and oxidative steam reforming (OSR) was studied applying microchannel testing reactors. The product composition was determined at a steam to carbon ratio (S/C) of 4.0, reaction temperatures between 625 °C and 725 °C and atmospheric pressure at volume hourly space velocities (VHSV) of the feed between 100 and 300 N L/(g_{cat} h). Catalysts with different rhodium loading were prepared by two different preparation methods (conventional impregnation and separate nanoparticle synthesis) and compared with regard to their activity and selectivity. All the catalysts were characterized using the following techniques: N_2 physisorption, temperature programmed reduction (TPR), transmission electron microscopy (TEM), X-ray diffraction (XRD), and X-ray photoelectron spectroscopy (XPS). Under all experimental conditions full conversion of ethylene glycol was achieved over the samples containing 2.5% and 5% Rh prepared by the impregnation method, equilibrium selectivity towards CO and CO_2, lowest selectivity towards CH_4 and lowest formation of by-products such as CH_3CHO and C_2 hydrocarbons. The other catalysts showed lower activity. The superior performance of the catalysts prepared by the impregnation method is supported by the measured higher rhodium dispersion of these samples.

1. Introduction

Hydrogen production from renewable sources and its utilization as a fuel for fuel cells is a promising way to minimize the actual dependence on fossil fuels. This dependence should be gradually reduced not only due to the fossil fuels depletion, but also owing to the environmental problems that entail their utilization. The challenge lays in the development of the most efficient, economical and environmentally friendly hydrogen production route. Thus, the energy conversion should be based on sustainable energy carriers in order to solve the concerns of environmental pollution and to ensure availability. In this context, the use of bio-renewable organic sources such as polyalcohols, in an intensified process through the use of a microstructured reactor seems to be a promising alternative [1,2].

The reforming of biomass-derived oxygenates such as ethanol or glycerol has been deeply studied. However, in the case of ethylene glycol, few studies have been addressed most of them focusing on aqueous phase reforming (APR). Ethylene glycol (EG) can be produced directly and efficiently via catalytic hydrogenation of cellulose or cellulosic biomass derived oxygenated compounds [3]. Cellulose, as the most abundant component of biomass (accounting for 35–50%), is being considered as a promising alternative to fossil resources [4]. In addition, EG is the most abundant molecule of compounds derived from the catalytic conversion of cellulose, accounting for more than 70% of cellulose derivatives, thus making EG a renewable and available energy carrier [5,6]. The group led by Prof. Dr. Tao Zhang reached full cellulose conversion and 61.0% EG yield by using a carbon supported tungsten carbide catalyst loaded with 2% of nickel [7,8] and lower conversions and yields by using other type of catalysts [9].

Therefore, the renewable and non-volatile nature makes EG an attractive feedstock for hydrogen production via steam reforming. Steam reforming is the preferred route for the conversion of biomass-derived oxygenates because the water is present in the feed already as described above and because steam reforming promises high efficiency in terms of higher hydrogen production yields [10,11]. The operation under SR conditions requires energy supply in order to achieve the reaction temperature and to feed the endothermic reaction. However, this fact is counterbalanced by the possibility to operate at atmospheric pressure which makes this process more attractive, easier and safer than APR [12].

Regarding the catalysts used, nickel [13,14], noble metal [10,15,16] and bimetallic catalysts [12,17] were studied in the APR process. In the case of the gas phase EG reforming, few investigations were found in the literature [3,7] which applied Ni based

* Corresponding author. Tel.: +34 946017297.
E-mail address: urko.izquierdo@ehu.es (U. Izquierdo).

0926-3373/$ – see front matter © 2014 Elsevier B.V. All rights reserved.
http://dx.doi.org/10.1016/j.apcatb.2014.01.012

catalysts, inert sand (SiO_2) or natural olivine. However, in the open literature to our knowledge, only Davda et al. [13] used Rh supported on SiO_2 for APR. However, Rh is known to be an excellent catalyst for steam reforming of all kind of fuels [2,10]. In this work catalysts supported by α-alumina were designed based upon two different preparation methods in order to compare their activity; namely a common wash-coating procedure with subsequent impregnation [18] (named as conventional method, *x*Rh-cm) and nanoparticle catalysts prepared according to a method described by Ashida et al. (named as nanoparticle catalysts, *x*Rh-np). Through this method, Rh nanoparticles are supposed to be obtained by doing a liquid phase reduction of the Rh^{3+} ion in ethanol solvent with polyvinylpyrrolidone (PVP) of the various molecular weights [19]. Finally, the support was chosen such that it had minimum acidity to reduce the risk of carbon formation of the catalyst.

These catalysts were tested under conditions of gas phase steam reforming of EG using microstructured reactors. It is well established that heat and mass transfer limitations are reduced when operating with microreactors and this fact makes them the most appropriate system to be used when fast and highly exothermic or endothermic reactions are studied. [20]. Additionally, the operation with microreactors also allows reaching much higher volume hourly space velocities (VHSV) owing to the improved mass transport in comparison with the conventional fixed bed reactors and this makes possible to intensify the process [21]. Furthermore, in a microchannel heat-exchanger the heat supply is possible in a much more efficient way compared to conventional technology.

2. Experimental procedure

2.1. Catalysts preparation and impregnation

For the preparation of the conventional catalysts, Rh ($RhCl_3 \cdot xH_2O$, Alfa Aesar, Johnson Mathey Company) was dissolved in 10 mL of distilled water in order to achieved the intended loadings of 1.0, 2.5 and 5.0 wt% of Rh. Then, 5 g of α-alumina was added and after subsequent stirring, the mixture was left for three hours without stirring at room temperature. These samples are named below as 1.0 Rh-cm, 2.5 Rh-cm and 5.0 Rh-cm, respectively.

The nanoparticle catalysts were prepared by mixing distilled water and ethanol (1:10 (vol.)) as a first step. Then, PVP ($(C_6H_9NO)_x$, Sigma Aldrich Chemie) and certain amount of Rh was added (1:5.33 (wt)). The resulting mixture was refluxed at 80 °C during 3 h. After cooling the mixture under continuous stirring overnight, a rotary evaporator was used to remove the ethanol. Finally, the corresponding amount of α-alumina were added to the obtained solutions in order to achieved the same metal content, 1.0%, 2.5% and 5.0% of Rh, as for the conventional catalysts. After successive stirring, the mixture was left for three hours without stirring at room temperature. These samples are named below as 1.0 Rh-np, 2.5 Rh-np and 5.0 Rh-np, respectively.

After the preparation described above, all catalysts were calcined at 450 °C for 6 h. The catalysts coatings were performed applying a procedure described by Zapf et al. [18] in which polyvinyl alcohol (PVA), distilled water and acetic acid were added to the previously calcined catalysts.

Sandwich-type reactors were applied for the activity tests. The reactors have two platelets carrying 14 channels each with 500 μm width and 250 μm depth introduced by wet chemical etching, which have been described in previous studies [20,21]. After an initial calcination of the plates the catalyst suspension was coated onto the plates by distributing manually some suspension drops along the plate's channels and removing any excess suspension from the completely filled channels. Subsequently, calcination at 600 °C for 2 h was carried out. The described coating and calcinations step was repeated twice. In addition, a certain amount of suspension was also calcined in order to characterize the resulting catalysts powder with same properties as the coated samples.

After calcination the reactors including inlet and outlet capillaries were sealed by laser welding. They were put into a stainless steel block equipped with thermocouples and heating cartridges to adjust the desired reaction temperature as described previously [22].

2.2. Activity measurements

A lab scale set up was applied for the activity tests (see Fig. 1). A mixture of water and ethylene glycol with a Steam-to-Carbon (S/C) ratio of 4.0 was used for experiments conducted under conditions of SR. In the case of OSR experiments a synthetic air stream composed of 21% O_2 and 79% N_2 (vol.) was introduced to reach the targeted atomic O/C ratio of 0.15. The liquid feed mixture was placed in a tank under N_2 pressure as driving force for feeding a liquid mass flow controller (LMFC). Before starting the experiments, the reactor was by-passed until a stable feed composition was measured and the desired reactor temperature was reached. The desired conditions were normally achieved approximately after 30 min by-passing the reactor.

The obtained product composition was analyzed using an online mass spectrometer (MS) equipped with two heated inlet systems (20–200 °C), an Electron Ion Source, a Quadrupole analyzer, a Faraday and a secondary electron multiplier (SEM) Detector. Then, the effluent stream was cooled down, water and organic liquids were removed and permanent gases were analyzed by an online μ-GC (Varian CP-4900 Micro-GC) equipped with a heated sample line (30–110 °C) consisting of 4-channel modules with four independent injectors and capillary columns connected with TCD detectors.

All the catalysts were tested at atmospheric pressure. For SR experiments the effect of temperature was studied at 625, 675 and

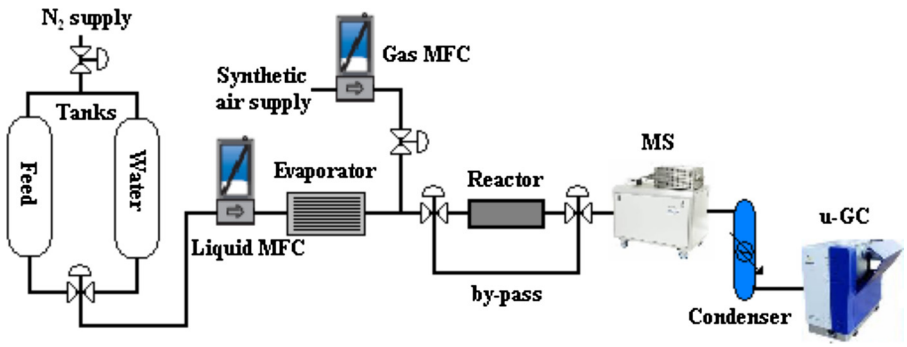

Fig. 1. Scheme of the experimental set up.

Table 1
Experimental conditions of the activity tests.

Process			SR			OSR		
Time progress (h)	1	2	3	4	5	6	7	8
Temperature (°C)	725	675	625	675			675	
VHSV (N L/h g_{cat})		200		300	100	100	200	300

725 °C at a volume hourly space velocity (VHSV) of 200 N L/(h g_{cat}). Then, at a constant temperature of 675 °C, the VHSV was modified to 100 and 300 N L/(h g_{cat}). In the case of OSR experiments, the effect of the VHSV was studied at a temperature of 675 °C. Each experimental condition was investigated for 1 h duration. Thus, the tests performed for each catalyst can be summarized as shown in Table 1.

The conversion of $C_2H_6O_2$ and the selectivity towards different carbon containing species $C_iH_jO_k$ were calculated from the following equations:

$$X_{C_2H_6O_2} = \frac{C_{0,C_2H_6O_2} - C_{1,C_2H_6O_2}}{C_{0,C_2H_6O_2}} \times 100\,[\%] \quad (1)$$

$$S_{C_iH_jO_k} = \frac{C_{1,C_iH_jO_k}}{\frac{2}{i} \times \left(C_{0,C_2H_6O_2} - C_{1,C_2H_6O_2}\right)} \times 100\,[\%] \quad (2)$$

where C_0 and C_1 are the concentration of the species at the reactor inlet (as determined by bypass measurements) and outlet, respectively, which were determined taking into account the volume changes of the reaction.

2.3. Catalyst characterization

Fresh and calcined catalysts were characterized by different techniques. The textural properties, BET surface area, pore volume and diameter of the calcined and outgassed (at 573 K for 3 h) catalysts were evaluated by means of N_2 adsorption obtained at 77 K using an Autosorb 1C-TCD. The specific surface area S_{BET} was calculated using the Brunauer–Emmett–Teller (BET) method while the total pore volume, V_p, and mean pore radius, P_r, were derived using the Barrett–Joyner–Halenda (BJH) method.

Temperature programmed reduction (TPR) measurements were performed in order to determine the reducible species formed during the calcination of the catalysts, and the reduction temperature. These analyses were conducted using an Autosorb 1C-TCD apparatus which was equipped with a thermal conductivity detector. A continuous flow of 5% H_2/Ar (40 N mL/min) was passed over 100 mg of calcined catalyst powder, and the temperature was increased from room temperature to 1273 K at a rate of 5 K/min. All the samples were previously outgassed at 573 K during 30 min.

Transmission electron micrographs were acquired on a Philips CM 200 transmission electron microscope (TEM) at an acceleration voltage of 200 kV with a LaB_6 filament. Typically, a small amount of sample was suspended in pure ethanol, sonicated and dispersed over a Cu grid with a carbon coated cellulose acetate–butyrate holey film. TEM images were recorded using a 4k × 4k TVIPS CCD camera at different magnifications.

Using PHILIPS X'PERT PRO automatic diffractometer X-ray powder diffraction (XRD) patterns were collected. The operation was carried out at 40 kV and 40 mA, in theta–theta configuration, secondary monochromator with Cu-$K\alpha$ radiation (λ = 1.5418 Å) and a PIXcel solid state detector. The samples were mounted on a zero background silicon wafer fixed in a generic sample holder. Data were collected from 20° to 70° 2θ (step size = 0.026 and time per step = 625 s) at RT. Using this technique, apart from identifying the species of the catalysts, the calculation of their particles size by the Scherrer equation was carried out.

Finally, X-ray photoelectron spectroscopy (XPS) technique was used to evaluate the surface characteristics of the fresh and tested catalysts. The measurements were carried out with a SPECS system (Berlin, Germany) equipped with a Phoibos 150 1D-DLD analyser and an Al $K\alpha$ ($h\upsilon$ = 1486.6 eV) X-ray source. The analysis of the catalysts components was carried out at the following experimental conditions: step energy of 1 eV, dwell time of 0.1 s and pass energy of 40 eV. Thereafter, a detailed scan of the detected compound was performed under the following conditions: step energy of 0.1 eV, dwell time of 0.1 s, pass energy of 20 eV and with an outlet electron angle of 90°. The obtained spectra were adjusted using CasaXPS 2.3.16 software which modelled the Gauss–Lorentzian contributions, after a background subtraction.

Table 2
Catalysts textural properties.

Catalyst	S_{BET} (m^2/g)	P_v (cm^3/g)	P_r (Å)
α-Al_2O_3	10.6	0.013	49
1.0 Rh-np	10.4	0.073	140
2.5 Rh-np	12.1	0.085	141
5.0 Rh-np	15.1	0.113	150
1.0 Rh-cm	10.3	0.083	161
2.5 Rh-cm	11.4	0.067	118
5.0 Rh-cm	12.3	0.080	130

BET surface area, S_{BET}; pore volume, P_v; and Pore radius, P_r.

3. Results and discussion

3.1. Characterization results

3.1.1. Textural properties, BET

The textural properties of fresh calcined catalysts are shown in Table 2. Taking into account that a surface area of 10.6 m^2/g was measured for the bare α-alumina, the rest of the catalysts showed increased surface area due to the Rh incorporation. Comparing among the catalysts, higher surface areas were obtained for the samples prepared by the nanoparticle method. A similar increase of the catalysts surface area was also reported in [23,24]. As far as the other measured parameters are concerned, increased pore size and pore volume were observed.

3.1.2. Temperature programmed reduction, TPR

TPR profiles of the fresh calcined catalysts are shown in Fig. 2. For each TPR analysis, the same amount of catalyst was used in order

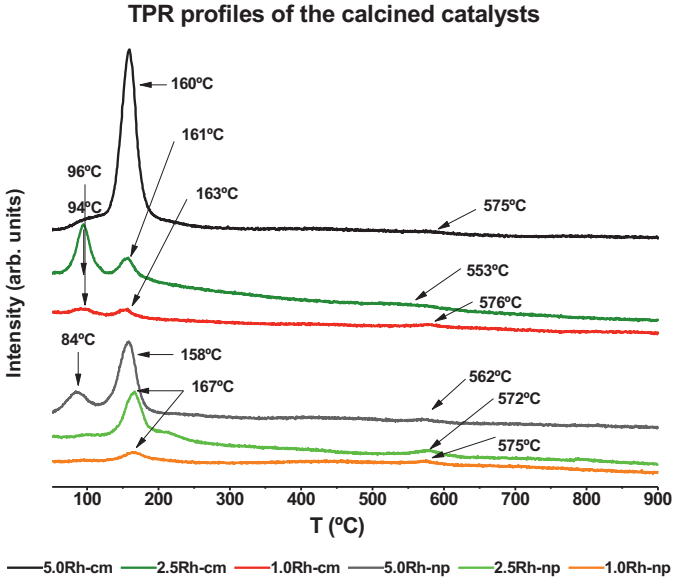

Fig. 2. TPR profiles of the calcined catalysts.

Table 3
Fresh calcined and tested catalysts, binding energies of Al 2p and Rh $3d_{5/2}$ core levels, atomic concentrations and Rh^0 and Rh^{3+} proportions (in parenthesis).

Catalyst	Fresh catalysts				Tested catalysts					Atomic ratios		
	Al 2p [eV, (%)]	Rh 3d [%]	Rh^{3+} [eV, (%)]	Rh^0 [eV, (%)]	C [%]	Al 2p [eV, (%)]	Rh 3d [%]	Rh^{3+} [eV,(%)]	Rh^0 [eV, (%)]	Rh/Al Theor.	Rh/Al fresh	Rh/Al tested
1.0 Rh-cm	72.9 (32.5)	0.94	308.9 (81.2)	307.3 (18.8)	86.2	74.2 (2.9)	0.76	308.8 (20.9)	307.4 (41.4)	0.005	0.03	0.06
2.5 Rh-cm	73.0 (33.1)	1.98	308.5 (78.8)	307.2 (31.2)	59.0	74.3 (13.6)	0.83	308.5 (21.4)	307.5 (37.4)	0.013	0.06	0.06
5.0 Rh-cm	73.4 (30.6)	2.75	308.5 (84.4)	307.4 (15.6)	60.1	74.2 (10.1)	0.63	308.8 (35.7)	307.6 (28.2)	0.026	0.09	0.26
1.0 Rh-np	73.5 (35.1)	1.51	308.9 (63.2)	307.2 (36.8)	72.5	74.4 (6.8)	0.44	308.7 (27.8)	307.4 (34.2)	0.005	0.04	0.06
2.5 Rh-np	72.8 (30.5)	3.15	308.3 (67.8)	307.2 (32.2)	83.2	76.1 (5.9)	0.74	308.8 (41.8)	307.4 (12.7)	0.013	0.10	0.12
5.0 Rh-np	73.3 (26.9)	4.89	308.2 (62.6)	307.2 (37.4)	86.7	74.7 (4.6)	0.59	n.d	n.d.	0.026	0.18	0.13

Theoretical, fresh and tested (After the tests specified in Table 1) catalysts surface atomic ratios.

to compare their reduction peaks. Therefore, as it can be observed in the figure, the size of the reduction peaks, proportional to the H_2 required for the species reduction, increased with the Rh metal load for both types of prepared catalysts. However, a considerably higher reduction peak was measured for the 5.0 Rh-cm catalysts, which can be related to the higher amount of reducible species. (This is confirmed by the XPS analyses carried out. See Table 3.)

The main reduction peaks, appear between 158 and 167 °C. In addition, smaller reduction peaks were detected at lower reduction temperatures (between 84 and 96 °C). For the 2.5 Rh-cm catalyst, the peak at the low temperature is the highest. It has been reported that these peaks correspond to a three-dimensional RhOx phase (large particles) and two-dimensional surface RhOx phase species at low and high temperatures, respectively [23,25]. The low temperature peaks are assigned to the reduction of RhOx species over the alumina surface and the other one, at higher temperature, to the RhOx species placed in the interface metal-support [26]. If the deconvolution of the peaks is carried out, for all the catalysts, except to the 2.5 Rh-cm, a better reducibility of the RhOx species placed in the interface metal-support is observed. In the case of the 2.5 Rh-cm catalysts, as the highest reduction peak is located at 94 °C, a major reduction of the RhOx species over the alumina surface occurred. Attending to the activity results described in Section 3.2, for this catalyst stable conditions and good activity results were achieved.

Apart from the described peaks, smaller interactions were detected at temperatures between 553 and 576 °C. These peaks can correspond to the strong interaction between the Rh and the α-alumina [27]. Finally, a different behaviour was noticed for the 2.5 Rh-np catalyst when a small peak at around 210 °C was detected. In addition, for this catalyst no peak was detected at the lowest temperature.

3.1.3. Transmission electron microscope TEM

In Fig. 3, the obtained TEM micrographs are collected. Using this technique, the particle sizes and dispersion differences between the two types of catalysts were observed. According to the obtained micrographs, particle aggregates were observed for the 5.0 Rh-np catalyst. When independent particles sizes were measured for this catalyst, most of them ranged between 4 and 6 nm and also few ranged from 10 to 15 nm. In the case of its homologous 5.0 Rh-cm catalyst, a better dispersion of the particles and more homogeneous size distribution was observed. However, more particles in the size range of 10–15 nm were measured in the micrograph of the latter catalyst. For the 2.5 Rh-np catalyst a lower density of particles

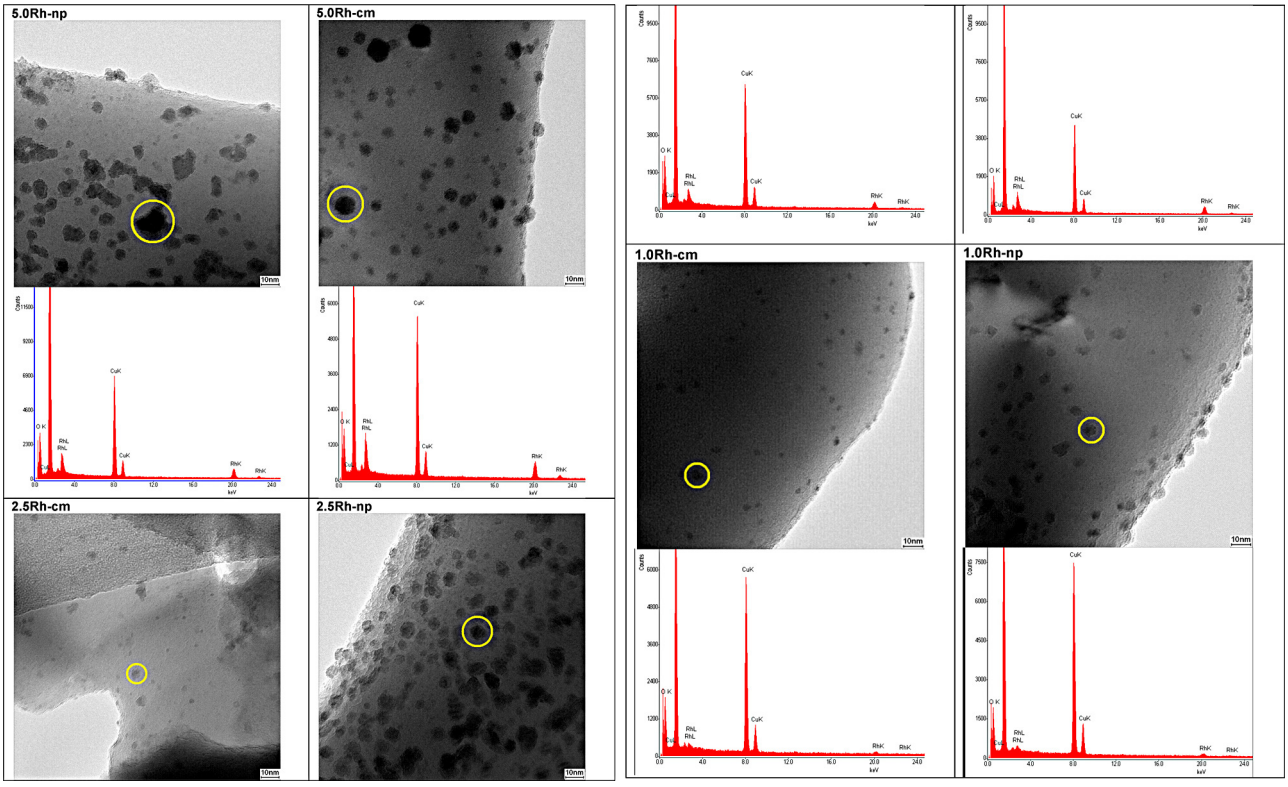

Fig. 3. TEM micrographs of the calcined catalysts. Scale bar = 10 nm.

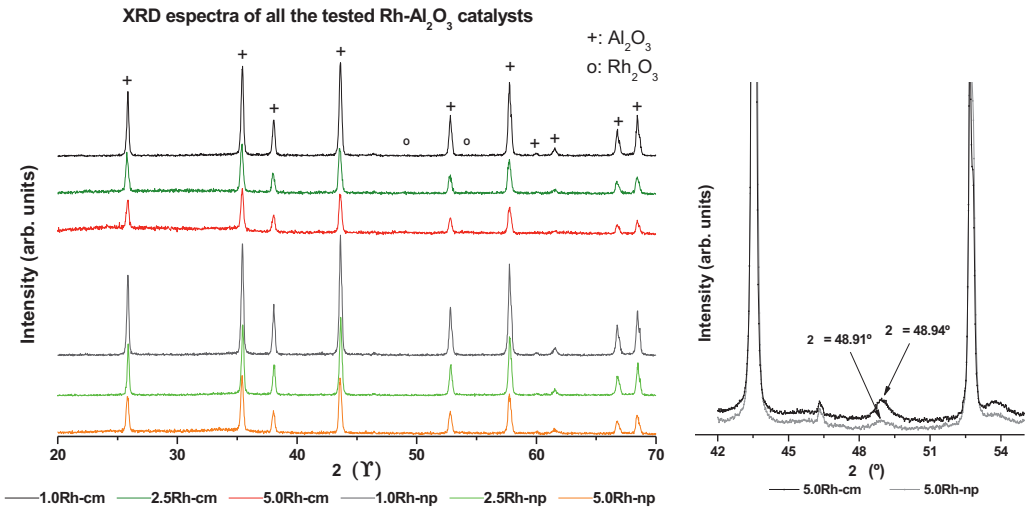

Fig. 4. XRD spectra of the Rh catalysts (left); Magnified XRD spectra for the 5 Rh-cm and np catalysts (right).

was observed with a majority between 4 and 6 nm, but also few between 10 and 15 nm. For this catalyst no particle aggregates were observed. In the case of its counterpart prepared by impregnation, for the 2.5 Rh-cm catalyst even lower particle density was observed and all particles were smaller than 5 nm. Finally, for the 1.0Rh catalysts the lowest particles density was observed. Comparing both catalysts, bigger particles were measured for the 1.0 Rh-np catalyst, ranging between 3 and 6 nm than for the 1.0 Rh-cm, for which all the observed particles were smaller than 4 nm. Thus, although the dispersion has not been analytically measured by H_2 pulse chemisorptions, a good dispersion of small noble metal particles is observed especially for the samples prepared by the impregnation method.

3.1.4. X-ray diffraction XRD

The obtained XRD spectra for the fresh calcined catalysts are shown in Fig. 4. The α-Al_2O_3 was perfectly identified (marked by the + symbol in the figure) by the corresponding peaks among the measured 2θ positions (Corundum, Powder Diffraction File (PDF): 01-075-0783). In the case of Rh species, the rhodium oxide contributions (Distinguished by the º symbol in the figure) should appear at 48.97° and 53.89° (PDF: 01-071-2084) in the measured 2θ region. However, only very small peaks were detected.

Accurate measurements were carried out to distinguish the peaks that correspond to the rhodium oxide, in order to calculate the particles size by the Scherrer equation. Therefore, in the right side of Fig. 4, magnified spectra obtained for the 5.0 Rh-cm and 5.0 Rh-np catalysts are shown. With these spectra, rhodium oxide contributions at 48.49° and 48.91°, respectively, were detected. As a result, rhodium oxide particles sizes of 15 nm for the 5.0 Rh-cm and 10 nm for the 5.0 Rh-np catalyst were estimated using the Scherrer equation. These results are in good agreement with the particle sizes observed in the TEM micrograph, taking into account that also smaller particles were observed. For the samples with lower Rh content, no peaks were detected. This only could be explained due to the limitations of the technique regarding the crystalline particles sizes (a particle size below 5 nm cannot be detected) which is also in good agreement with the micrographs obtained by TEM. In addition, the technique is also limited by the amount of the metal in the catalysts, which is low in the case of the 1.0 Rh and 2.5 Rh catalysts.

3.1.5. XPS

XPS analysis was carried out to determine the chemical composition of the catalysts surface and to better understand the nature of interaction between the dispersed metal species and the support. The results of the fresh calcined and tested catalysts are summarized in Table 3. In the case of the tested catalysts, the measurements were carried out after the conditions specified in Table 1.

For the XPS results interpretation, the peak that corresponds to C_{1s} was used in order to standardize all the spectra obtained for both fresh reduced and spend catalysts. Focusing on the results obtained for the fresh reduced catalysts, two main differences can be observed if cm and np catalysts are compared; the total Rh atomic concentration (Rh_{3d}) and the metallic Rh atomic concentration (Rh^0) were both higher for the np-catalysts than for their homologous cm ones. For both type of catalysts the Rh_{3d} increased with the Rh theoretical amount, but in the case of the Rh^0, no clear tendency was observed. Thus, more active sites were supposed to be available for the np fresh reduced catalysts. Attending to the columns that correspond to the catalysts tested, the results obtained were not expected when compared with those obtained for the fresh calcined samples, but they agree with the activity results obtained (see Section 3.2). For all the np-catalysts very high carbon atomic

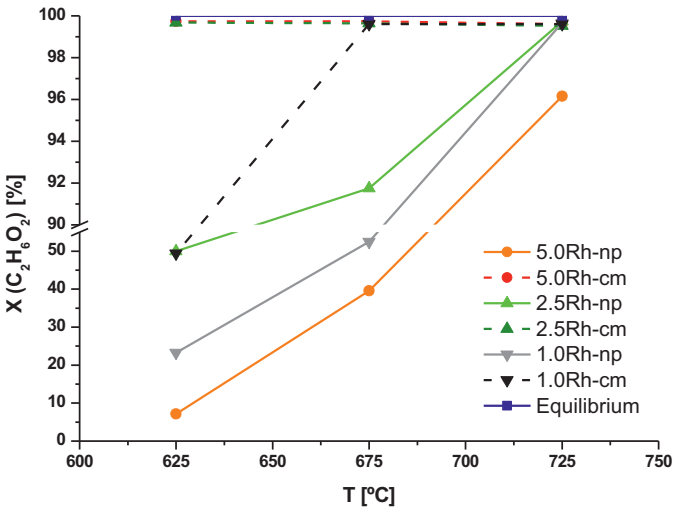

Fig. 5. Conversion vs. reaction temperature as obtained for all catalysts under investigation under conditions of SR.

concentration was measured. Due to this fact, the Rh_{3d} detected for these catalysts was very low and as a consequence, Rh^{3+} or Rh^0 could not to be detected for the 5 Rh-np catalysts by this technique. In the case of the rest of np-catalysts, although a high carbon atomic concentration, Rh^{3+} and Rh^0 species were detected as specified in the table. For the cm-catalysts, higher Rh_{3d} were measured due to the apparently lower carbon deposition. For the 2.5 Rh-cm catalyst was measured the highest Rh_{3d} and also the highest Rh^0. According to the activity results obtained, the 5.0 Rh-cm and 2.5 Rh-cm catalysts showed the best performance. In addition, for all the tested catalysts a doublet at higher binding energies was detected, at 310.4 and 315.0 eV, respectively. According to those binding energies, the

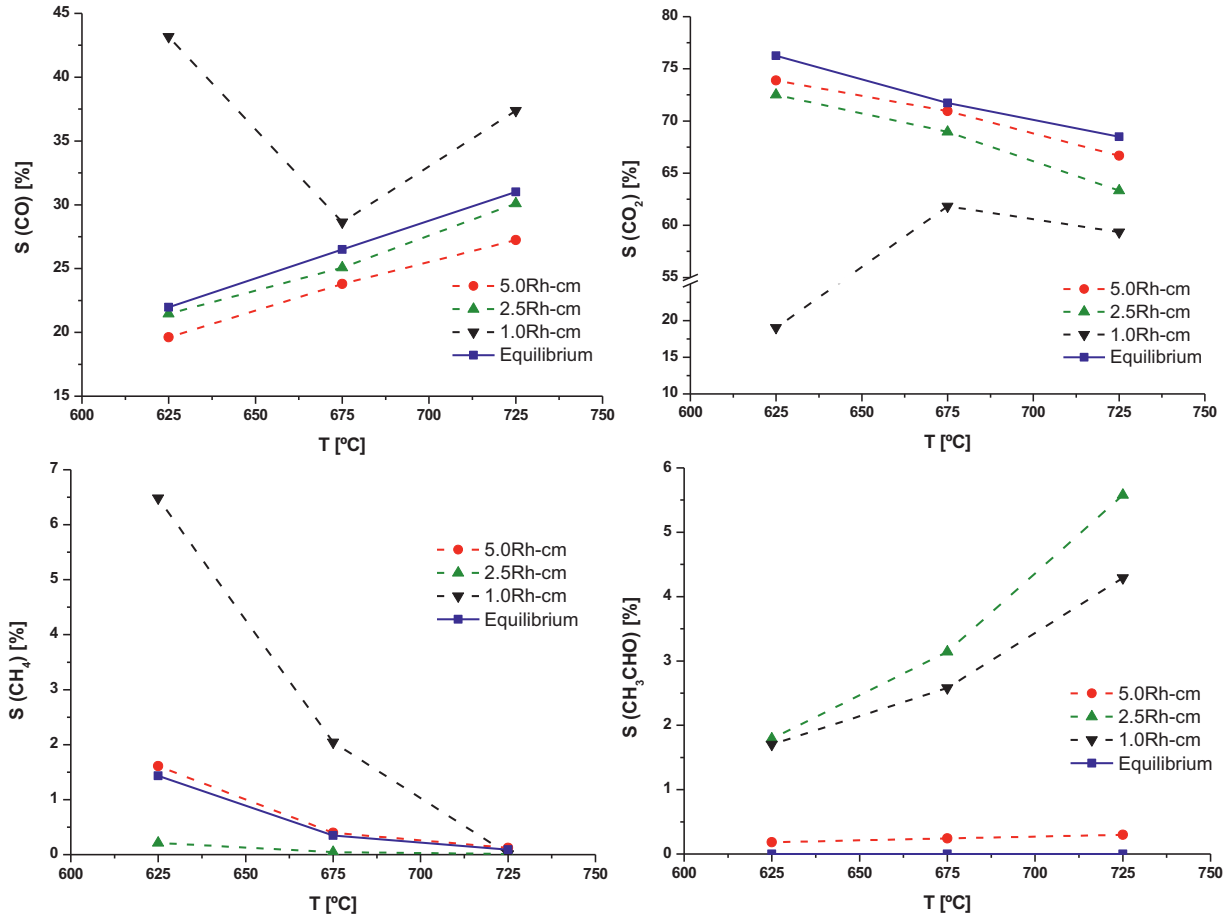

Fig. 6. Selectivities vs. reaction temperature as obtained for the catalysts prepared according to the conventional method (cm) under conditions of SR; (a) top left: CO selectivity; (b) top right: CO_2 selectivity; (c) bottom left: CH_4 selectivity; (d) bottom right: CH_3CHO selectivity; the values as calculated for the thermodynamic equilibrium of the reaction mixture are included.

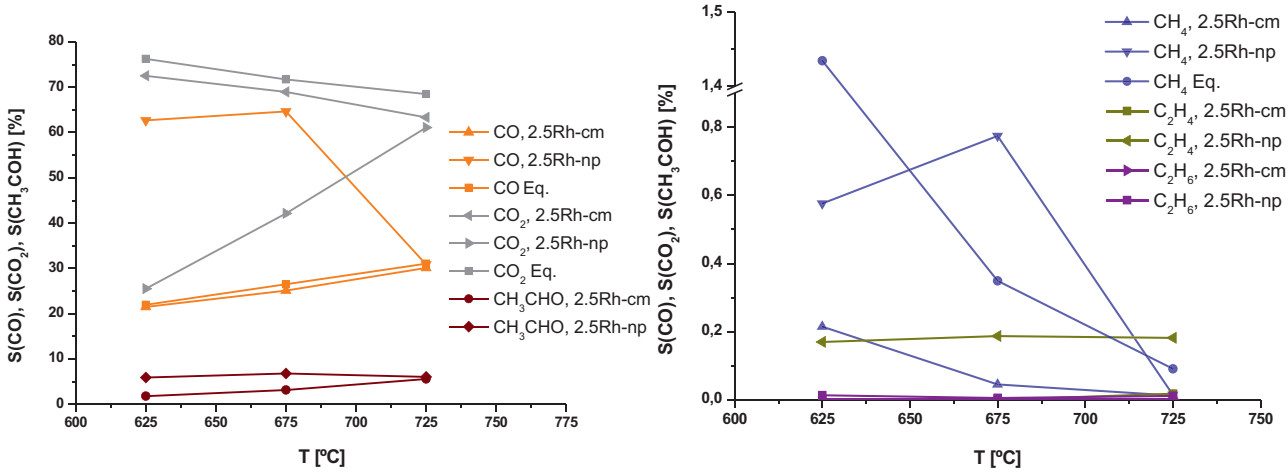

Fig. 7. Selectivities vs. reaction temperature as obtained for the catalysts containing 2.5 wt% Rh prepared according to the conventional method (cm) and the nanoparticle method (np) under conditions of SR; (a) left: CO, CO_2 and CH_3CHO selectivity; for CO and CO_2 the values as calculated for the thermodynamic equilibrium of the reaction mixture are included; (b) right: CH_4, C_2H_4,C_2H_6 selectivity; for CH_4 the values as calculated for the thermodynamic equilibrium of the reaction mixture are included.

doublet could be attributed to the Rh but this has not been reported in the literature neither in any data base. Finally, higher Rh/Al ratios were measured for the fresh np-catalysts than for the cm catalysts, as expected. Each catalyst showed higher Rh/Al ratio after testing, apart from the 5 Rh-np catalysts, which could originate from the preferential carbon deposition on the alumina surface.

3.2. Results from activity testing

Fig. 5 shows the conversion of EG as obtained over the catalysts under investigation at different reaction temperature and under conditions of SR. It is obvious that cm-catalysts show much higher activity. Apart from the sample 1.0 Rh-cm, full conversion was always achieved while the np-catalysts showed much lower activity. While 1.0 Rh-np sample showed lower activity compared to the sample 2.5 Rh-np as expected, the activity of the 5.0 Rh-np sample is even lower, which is not explained by the catalyst characterization described above.

For the cm samples, the selectivity towards the by-products is compared in Fig. 6. While the selectivity towards CO (see Fig. 6a) and CO_2 (see Fig. 6b) is close to the thermodynamic equilibrium for the samples 2.5 Rh-cm and 5.0 Rh-cm, the 1.0 Rh-cm sample shows higher selectivity towards CO (the primary product of steam reforming) and lower selectivity towards CO_2, because the water–gas shift activity of the catalyst is insufficient. The selectivity towards CH_4 (see Fig. 6c) shows a more complicated pattern. The 5.0 Rh-cm sample shows values close to the thermodynamic equilibrium of the methanation reaction. For the 2.5 Rh-cm sample the values are lower than those expected from thermodynamics, which is attributed to a low methanation activity of the catalyst. As the result, no CO is converted to methane. The 1.0 Rh-cm sample obviously released methane as a result of incomplete conversion of EG during steam reforming and has likely no methanation activity at all. Acetaldehyde is formed as by-product mostly over the 2.5 Rh-cm and 5.0 Rh-cm samples (see Fig. 6d).

Fig. 7 shows a comparison of the samples contaning 2.5% Rh prepared by the cm and np methods (2.5 Rh-cm and 2.5 Rh-np). The np catalyst shows a much higher CO selectivity, lower CO_2 selectivity and also higher acetaldehyde selectivity (see Fig. 7a). The methane selectivity of the np catalyst is higher as well as its selectivity towards other undesired by-products, namely higher hydrocarbons

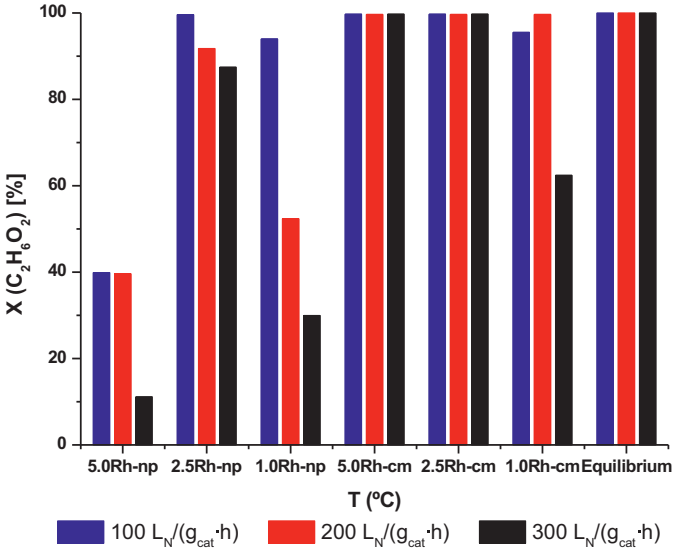

Fig. 8. Conversion as obtained for all catalysts under investigation at a reaction temperature of 675 °C under conditions of SR at different VHSV.

such as ethylene and ethane, which proves once more the inferior performance of this catalyst type (see Fig. 7b).

Fig. 8 shows a comparison of the conversion as obtained for all catalysts at different space velocities (VHSV), which documents the inferior performance of the np catalysts, showing dramatically lower conversion at higher feed flow rates.

Fig. 9 shows the selectivities towards methane, ethylene and acetaldehyde as determined under conditions of SR and OSR at all samples under investigation. The methane formation is lowest for the cm samples containing 2.5% Rh and more. It is suppressed by lower space velocity and oxygen addition in most cases (see Fig. 9a and b). Similar observations were made with respect to ethylene, while no ethylene was formed at the cm samples containing 2.5% and 5% Rh (see Fig. 9c and d). The results are less straight-forward for acetaldehyde (see Fig. 9e and f). No clear effect of increased feed flow rate could be observed, while the oxygen addition obviously increased the acetaldehyde formation unexpectedly.

Table 4
Hydrogen production rates at the tested conditions.

Catalyst: amount	$C_2H_6O_2$ SR				$C_2H_6O_2$ OSR	
	VHSV = 200 N L/(h g_{cat})		T = 675 °C		T = 675 °C	
	T (°C)	H_2 flow (L/(g_{cat} h))	VHSV (L/(g_{cat} h))	H_2 flow (L/(g_{cat} h))	VHSV (L/(g_{cat} h))	H_2 flow (L/(g_{cat} h))
1.0 Rh-np: 0.0166 g	725	75.4			300	51.5
	675	43.6	300	40.6	200	34.4
	625	20.9	100	32.7	100	41.4
2.5 Rh-np: 0.0161 g	725	95.8			300	79.2
	675	77.8	300	96.4	200	61.8
	625	46.4	100	38.8	100	41.7
5.0 Rh-np: 0.0145 g	725	81.0			300	20.3
	675	29.0	300	15.4	200	15.0
	625	7.2	100	12.5	100	10.4
1.0 Rh-cm: 0.0160 g	725	91.5			300	50.0
	675	91.8	300	6.8	200	34.3
	625	38.9	100	3.2	100	24.4
2.5 Rh-cm: 0.0171 g	725	94.9			300	**146.6**
	675	**99.9**	300	**150.69**	200	**119.4**
	625	**101.7**	100	**50.83**	100	**48.9**
5.0 Rh-cm: 0.0164 g	725	**97.7**			300	133.3
	675	98.9	300	148.4	200	82.7
	625	98.7	100	49.5	100	36.7

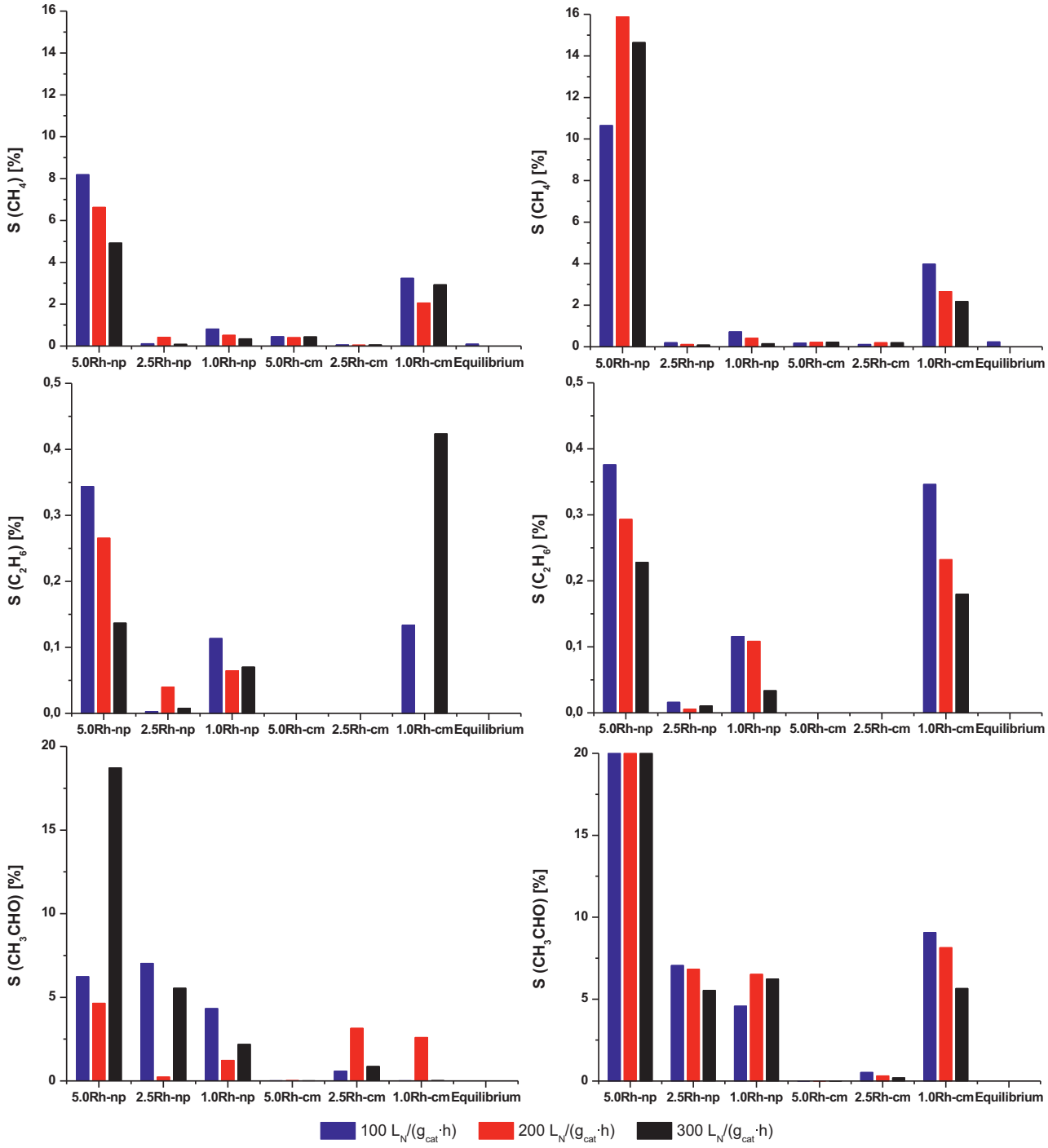

Fig. 9. Selectivities at different VHSV as obtained for all catalysts at 675 °C reaction temperature under conditions of SR and OSR; (a) top left: CH_4 selectivity (SR); (b) top right: CH_4 selectivity (OSR) (c) center left: C_2H_6 selectivity (SR); (d) center right: C_2H_6 selectivity (OSR); (e) bottom left: CH_3CHO selectivity (SR); (f) bottom right: CH_3CHO selectivity (OSR).

Fig. 10 shows the hydrogen molar composition measured for the SR process carried out at different temperatures. Higher hydrogen molar concentrations were measured at higher temperatures for the np samples. In the case of both 2.5 Rh-cm and 5.0 Rh-cm samples, the hydrogen composition measured followed the equilibrium predictions. However, for the samples with lower metal content, the measured hydrogen composition was lower at the lowest temperature.

In Table 4 the calculated hydrogen production rates are shown for the different experimental condition studied. As expected after the results presented, the 2.5 Rh-cm catalyst reached the highest hydrogen production rates under all the conditions tested with the

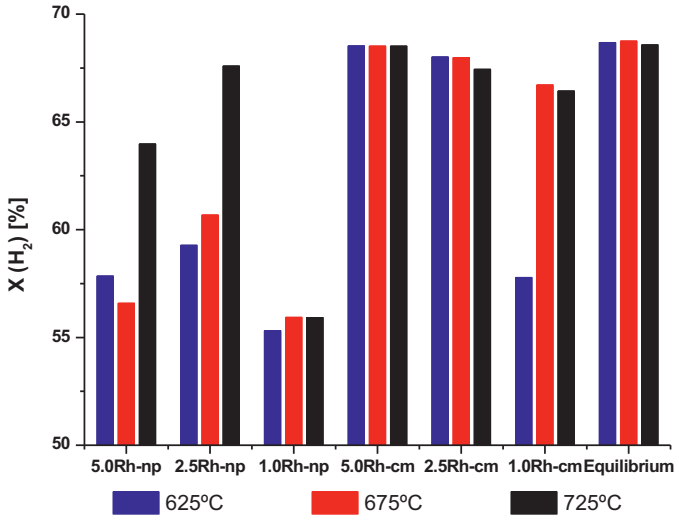

Fig. 10. Measured hydrogen molar compositions under SR at different T (Dry basis).

exception of SR at 725 °C, and surprisingly the 5.0 Rh-np sample the lowest.

4. Conclusions

Rh containing catalysts were prepared by different preparation methods and tested for their activity in steam reforming and oxidative steam reforming of ethylene glycol. While the samples prepared by a conventional impregnation method showed generally higher activity compared to catalysts prepared from Rh nanoparticles, all samples suffered from by-product formation of species such as acetaldehyde, ethane and ethylene regardless if oxygen was added to the feed or not. In future investigations how the catalyst activity can be further improved and by-product formation can be suppressed by addition of ceria or lanthana to the catalyst formulation will be investigated. In addition, the catalysts stability will be also investigated through long term experiments.

References

[1] D.J.M. De Vlieger, A.G. Chakinala, L. Lefferts, S.R.A. Kersten, K. Seshan, D.W.F. Brilman, Appl. Catal., B 111 (2012) 536–544.
[2] G. Kolb, Chem. Eng. Proc. 65 (3) (2013) 1–44.
[3] S. Li, C. Zhang, P. Zhang, G. Wu, X. Ma, J. Gong, Phys. Chem. Chem. Phys. 14 (2012) 4066–4069.
[4] Y. Zhang, A. Wang, T. Zhang, Chem. Commun. 46 (2010) 862–864.
[5] H.D. Kim, T.W. Kim, H.J. Park, K.E. Jeong, H.J. Chae, S.Y. Jeong, Int. J. Hydrogen Energy 37 (2012) 12187–12197.
[6] H.Y. Law, M.C. Kung, H.H. Kung, Catal. Today 136 (2008) 40–45.
[7] N. Ji, T. Zhang, M. Zheng, A. Wang, H. Wang, X. Wang, et al., Angew. Chem. Int. Ed. 47 (2008) 8510–8513.
[8] N. Ji, T. Zhang, M. Zheng, A. Wang, H. Wang, X. Wang, et al., Catal. Today 147 (2009) 77–85.
[9] G. Zhao, M. Zheng, A. Wang, T. Ahang, Chin. J. Catal. 31 (2010) 928–932.
[10] P.N. Kechagiopoulos, S.S. Voutetakis, A.A. Lemonidou, I.A. Vasalos, Catal. Today 127 (2007) 246–255.
[11] G. Kolb, Fuel Processing for Fuel Cells, Wiley-VCH, Weinheim, 2008.
[12] G.W. Huber, J.W. Shabaker, S.T. Evans, J.A. Dumesic, Appl. Catal., B 62 (2006) 226–235.
[13] R.R. Davda, J.W. Shabaker, G.W. Huber, R.D. Cortright, J.A. Dumesic, Appl. Catal., B 43 (2003) 13–26.
[14] F. Xie, X. Chu, H. Hu, M. Qiao, S. Yan, Y. Zhu, et al., J. Catal. 241 (2006) 211–220.
[15] J.W. Shabaker, R.R. Davda, G.W. Huber, R.D. Cortright, J.A. Dumesic, J. Catal. 215 (2003) 344–352.
[16] J. Liu, B. Sun, J. Hu, Y. Pei, H. Li, M. Qiao, J. Catal. 274 (2010) 287–295.
[17] O. Skoplyak, M.A. Barteau, J.G. Chen, J. Phys. Chem. B 110 (2006) 1686–1694.
[18] R. Zapf, C. Becker-Willinger, K. Berresheim, H. Bolz, H. Gnaser, V. Hessel, et al., Chem. Eng. Res. Des. 81 (2003) 721–729.
[19] T. Ashida, K. Miura, T. Nomoto, S. Yagi, H. Sumida, G. Kutluk, et al., Surf. Sci. 60 (2007) 3898–3901.
[20] M. O'Connell, G. Kolb, R. Zapf, Y. Men, V. Hessel, Catal. Today 144 (2009) 306–311.
[21] U. Izquierdo, V.L. Barrio, J.F. Cambra, J. Requies, M.B. Güemez, P.L. Arias, et al., Int. J. Hydrogen Energy 37 (2012) 7026–7233.
[22] G. Kolb, R. Zapf, V. Hessel, H. Löwe, Appl. Catal., A 277 (2004) 155–166.
[23] M. Ocsachoque, F. Pompeo, G. Gonzalez, Catal Today 172 (2011) 226–231.
[24] M. Ghelamallah, P. Granger, Fuel 97 (2012) 269–276.
[25] Y. Li, X. Wang, C. Xie, C. Song, Appl. Catal., A 357 (2009) 213–222.
[26] I. Cuauhtémoc, G. Del Angel, G. Torres, C. Angeles-Chavez, J. Navarrete, J.M. Padilla, Catal. Today 166 (2011) 180–187.
[27] X. Karatzas, J. Dawody, A. Grant, E.E. Svensson, L.J. Pettersson, Appl. Catal., B 101 (2011) 226–238.